



A novel lung cancer detection adopting Radiomic feature extraction with Locust assisted CS based CNN classifier

P. Lavanya ^{a,*}, K. Vidhya ^b

^a Department of Electronics and Communication Engineering, Saveetha School of Engineering, Saveetha Institute of Medical and Technical Sciences, Thandalam, Chennai-602105, India

^b Department of Electronics and Communication Engineering, Saveetha School of Engineering, Saveetha Institute of Medical and Technical Sciences, Thandalam, Chennai-602105, India



ARTICLE INFO

Keywords:

Adaptive Wiener Filter
Cascaded KM-FCM Algorithm
Radiomics Feature Extraction
Locust Assisted CS based CNN

ABSTRACT

Cancer is regarded as one of the life-threatening diseases since it causes significant number of fatalities in every year. Among different cancer types, the lung cancer is considered as the most destructive type with largest mortality rate. Therefore, an effective and accurate technique for detecting the lung cancer is crucial for providing the adequate treatment on time. This study presents a novel deep learning-based lung cancer detection method. The technique of image processing comprises of four major phases. Initially, the pre-processing of input images is carried out with the implementation of Adaptive Wiener filter for successfully eliminating the noises in the image without making any edge loss. Then, the process of segmentation is executed using Cascaded K-means Fuzzy C-means (KM-FCM) algorithm. The stages of feature extraction and selection are carried out using Radiomics approach, which aids in the extraction and selection of meaningful features that facilitates cancer detection. The final stage of image processing is classification, which is accomplished by a novel Locust assisted Crow Search (CS) based Convolutional Neural Network (CNN) classifier. The proposed digital image processing technique displays an impressive performance in detecting lung cancer with an accuracy of 96.33%.

1. Introduction

The consequences of lung cancer is significantly greater than the other types of cancers as it causes severe health issues and increases the mortality rate in a wider range [1]. One of the most prevalent and deadly types of cancer is caused by abnormal and uncontrollably growing lung tissue cells. Although this cancerous development can originate in any area of the lungs, it usually does so from the cells that line the respiratory tract [2,3]. The cancer has to be detected in the early stage to recognize the existence of pulmonary nodules that cause tumour in the lung [4]. Generally, the lung cancer is diagnosed in final stages, which leads to failure in providing the necessary treatment on time and lessening the mortality rate of lung cancer. After the diagnosis of lung cancer, the average five-year survival rate is about 15% but it is possible to increase the five-year survival rate up to 70% if the lung cancer is identified in the early stages. Hence, the early clinical identification of lung cancer leads to improved survival rates [5]. Manually detecting tumour volumes in lung tissues is a highly complex and labour-intensive task due to the intricate processes involved. This method requires radiologists to

meticulously analyze numerous images from scans such as CTs or MRIs, attempting to identify and measure tumours. Such a task is not only time-consuming but also prone to human error. In contrast, image processing techniques offer a high level of precision and consistency, processing large volumes of imaging data rapidly, which is critical in timely and accurate cancer diagnosis. These technologies enhance the detection capabilities, particularly of small or early-stage tumours that are crucial for effective treatment planning and improved patient outcomes [6,7]. Thus, the detection of lung cancer is simplified by adopting image processing techniques. It includes the processing of image, which involves in generating an enhanced image by the extraction of relevant features [8].

The phases of an image processing technique include pre-processing, segmentation, feature extraction, feature selection and classification. In pre-processing, the filters are utilized to eliminate the speckle noise without eliminating significant features and edge informations. Initially, the linear filters are preferred for image pre-processing, which involves in altering the frequency spectrum of the signal. Because of the negligence of image and noise characteristics, it leads to blurring of contrast

* Corresponding author.

E-mail addresses: lavanyap780@gmail.com (P. Lavanya), vidhyak.sse@saveetha.com (K. Vidhya).

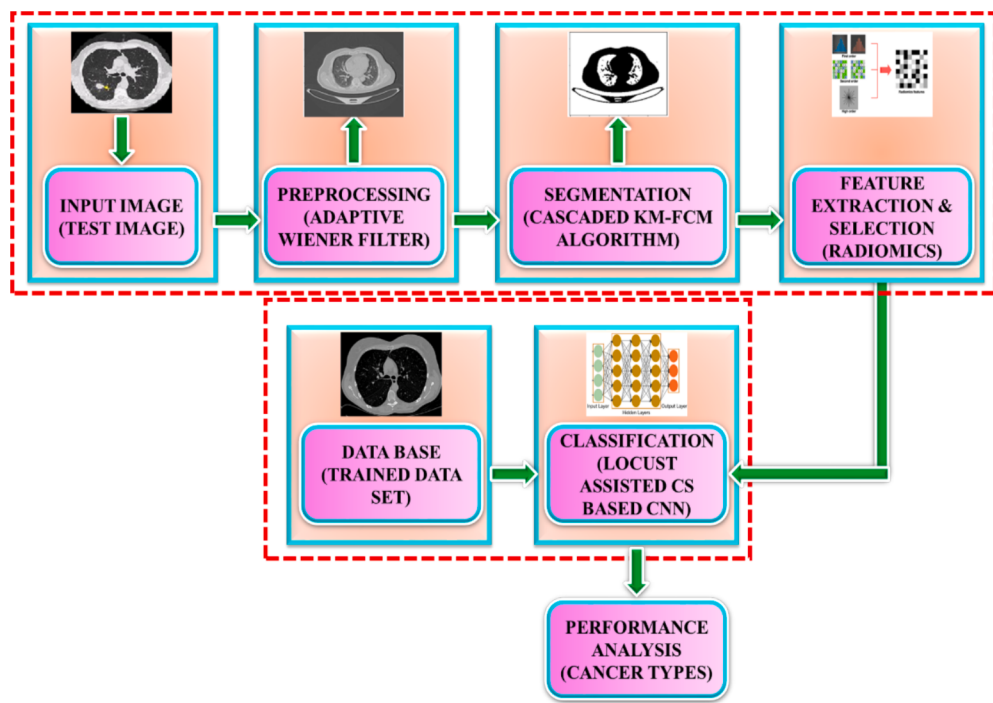


Fig. 1. Proposed Block Representation.

and edge field of images [9,10]. The Lee filter is another type of filter, which depends on the Linear Minimum Mean Squared Error (LMMSE) estimator. Though it performs despeckling of images, it demands the selection of similar pixels for guaranteeing the scene stationarity [11]. In recent times, the model-based filters are involved in image pre-processing for solving various inverse issues but these filters consume more time to solve those issues [12]. Conventional Wiener filters are also used for pre-processing the images, which provide optimized balance between smoothening of noise and inverse filtering. In this filtering, the periodical calculation of coefficients is performed, which subsequently adapts the filter with average image characteristics of the block [13,14].

Following the pre-processing stage, the segmentation of images is carried out as it is highly prerequisite for the medical image and computer vision analysis. The basic segmentation approaches are region-based and boundary-based techniques. These approaches fail to generate accurate segmented results and neglect details or resolution of images [15]. The classical fuzzy C-means approach is employed for the segmentation of images, which uses the fuzzy set for resolving the clustering issues. Though this approach is advantageous, it is computationally expensive [16]. Moreover, some of the fuzzy models lack the ability of correcting the bias field due to the non-consideration of spatial information [17]. In literature, the segmentation by K-means is widely used and this algorithm requires cluster validity indices for improved segmentation [18,19]. By cascading both the K-means and fuzzy C-means approaches, enhanced segmentation results are obtained in this work since the complete potential of both approaches is utilized in an efficient manner.

Following the segmentation phase, the feature extraction is necessary for accurately classifying the lesion malignancy to avoid unnecessary follow-ups and to reduce false positives [20]. The Contrast Limited Adaptive Histogram Equalization (CLAHE) results in better visualization for the segmentation of images but it possess poor variability [21]. The Independent Component Analysis (ICA) achieves better results in extracting features but faces potential restrictions [22]. Other feature extraction approach like Principal Component Analysis (PCA) perform the learning of low dimensional features in unsupervised manner but the latent discriminative data information is eliminated in

this approach [23,24]. The Radiomics has evolved as a powerful and promising approach for detecting cancer. It involves abundant quantitative features and high-throughput extraction [25]. The heterogeneity and potential microstructure are characterized by radiomics, which has the ability for identifying the location of lesions and providing improved detection performance [26].

The segmented image is further subjected to classification for detecting lung cancer. Machine Learning (ML) approaches are widely opted for the diagnosis of cancer but these methods concentrate individual properties like shape, texture and colour [27]. The unsupervised approaches for classification fail to generate accurate classification results because these approaches perform the classification of data without any prior knowledge [28]. Semi-supervised methods are also involved in the classification of images, which deliver optimal outputs with improved accuracy. Meanwhile, these methods demand complicated training process [29]. Among supervised learning approaches, traditional SVM classifier achieves classification outputs in a satisfactory manner but consumes more time and so it is practically unfeasible [30,31]. The Decision Tree [DT] models are also preferred for the classification processes these models have improved robustness and interpretability. However, these models are computationally expensive [32]. Due to the rapid progress of deep learning algorithms, Artificial Intelligence (AI) approaches are highly preferred for the analysis and classification of medical images. These approaches avoid invasive trauma in biopsy and performs the comprehensive analysis of malignant tumours [33,34].

For lung cancer detection, in [35], an optimized YOLO v3 architecture is employed. The model supports fast and accurate object detection and allows for efficient real-time processing. Despite its high accuracy, the model generates a notable number of false positives and false negatives, which is problematic in a clinical setting, causing missed diagnoses. In [36], YOLO v7 and VGG 16 are employed for identifying cancer and these methods enhances the diagnosis process by demonstrating promising accuracy in nodule classification. However, the risk of overfitting and limited interpretability are considered to be its major limitations. The optimized hybrid neural network model proposed in [37], improves feature learning and classification performance by using

sequential and feed-forward learning. However, the computational complexity of the hybrid model increases its training time. In [38], lung cancer is detected using stacked neural network. While this model shows high accuracy, its performance is limited on borderline and ambiguous cases.

Henceforth, the limitations of the existing works in the context of medical image analysis are addressed as follows: Initially, the existing pre-processing approaches, while straightforward, tend to neglect the specific characteristics of images and noise and are hindered by their time-consuming nature. Segmentation techniques fail to accurately capture detailed image resolutions and are computationally demanding. Feature extraction methods exhibit poor variability to the elimination of critical discriminative information. Classification stages also encounter significant hurdles, with machine learning approaches focusing narrowly on individual image properties and unsupervised methods lacking accuracy due to the absence of prior knowledge. The advent of deep learning and AI approaches marks a significant advancement, yet these technologies still grapple with issues related to interpretability, the requirement for extensive training data, and the risk of overfitting.

Considering the above factors, this work develops an enhanced image processing approach for the detection of lung cancer which contributes the following.

- The Adaptive Wiener Filter utilized for image denoising dynamically adjusts its output by accounting for the local variance within the image, thereby enhancing image quality by effectively reducing noise without compromising significant image details.
- Cascaded KM-FCM algorithm employed for segmentation ensures more precise outcomes by combining the complete potential of both methodologies.
- Feature Extraction through Radiomics is adopted for the extraction of features, which facilitates the efficient prediction of tumor characteristics. This approach harnesses a wide array of quantitative features, enabling a more detailed analysis and characterization of tumors.
- Classification is performed using Locust Assisted CS-based CNN which results in improved classification metrics, ensuring more accurate and reliable identification of tumour attributes.

This paper is structured as follows: section II presents a thorough explanation of the proposed approach; section III covers modeling; section IV comprises results and discussion; and section V concludes.

2. Proposed methodology

The procedure for identifying the lung cancer in the initial stage is highly essential for lessening the mortality rate of cancer in a wider range since most of the patients diagnosed with lung cancer have lost the life because of detecting the disease in the advanced stage. Hence, the present study proposes the image processing approach for identifying the occurrence of cancer in the early stage with optimum accuracy and maximum reliability. This approach's block diagram is remarkably portrayed in Fig. 1 for signifying the functioning measures of the introduced methodologies in an efficient manner.

The cancer affected lung image is taken as the input image, which is pre-processed in the initial stage with the assistance of an Adaptive Wiener Filter that involves in eliminating the unwanted noises in a suitable way and the denoised image is then segmented into multiple regions through the implementation of Cascaded KM-FCM algorithm for attaining disruption free accurate results. The features of these segmented images are then effectively extracted and selected by employing the Radiomics approach which performs the minimization of feature dimensionality. Then the selected features are significantly classified by implementing the Locust assisted CS based CNN classifier, which involves in classifying the images in accordance with the trained data set and delivers enhanced output in classifying the stages of cancer

with maximum accuracy. Due to its ability to accurately identify lung cancer even in its early stages, the proposed approach is therefore extremely relevant for the early detection of cancer without any complications. The working principles and designing measures of this entire approach is phenomenally detailed in the remaining section.

3. System Modelling

The stages in the process of detecting the lung cancer are remarkably explained in this section with prior analysis, which assists in validating the cumulative performance of the system in an effective way.

3.1. Pre-Processing

The necessity of pre-processing is highly essential in overall process of detecting the lung cancer as it aids in enhancing the input image by eliminating the unwanted noise contents and hence it is regarded as one of the mandatory steps to be carried out for obtaining optimal outcomes. The random unpredictable errors in the input image cause certain disruptions in accurately identifying the occurrence of lung cancer and so these errors have to be eliminated from the image by using an effective approach. These disruptions manifest as various types of noise, such as electronic interference during the image capture process, artifacts introduced during image transmission, or even variations due to differences in imaging equipment. Noise obscures the fine details and nuances within an image that are crucial for identifying the characteristics of lung cancer, such as the size, shape and edges of nodules. Noise can also disrupt the processes of segmentation and feature extraction by creating ambiguities in the boundaries of the lung and lesions, leading to inaccurate segmentation and the extraction of irrelevant or misleading features. Hence, an Adaptive Wiener Filter is significantly employed in this present study to attain a noise free image since it corrects the input image in consideration with the local variance of the image.

The operation of the Adaptive Wiener Filter in denoising images involves adjusting the filter's parameters based on the local image characteristics, specifically the local mean and variance. This filter is particularly adept at handling images corrupted by additive noise, where the objective is to estimate the original image from the noisy observation. It operates under the premise that the noise is zero-mean white Gaussian, allowing for a targeted reduction in mean squared error (MSE) between the original and the denoised image. The Adaptive Wiener Filter calculates local means and variances within a moving average window, adapting its response to the variance of the noise and the signal in each local area of the image. For areas with unexpected edges or high-frequency information, the filter employs adaptive weights to ensure that denoising preserves these crucial features. This adaptive weighting is crucial for maintaining image details and edges, making it superior for images where preserving edge integrity and high-frequency regions is vital.

This approach focuses on lessening Mean Squared Error (MSE) among original and restored images, which is regarded as the most significant characteristics of de-noising the image in an optimal manner. As it is highly beneficial in preserving the regions of high-frequency and image edges, the filtering capacity of this particular approach is comparatively optimal than others.

Filtering of signals affected by zero-mean white Gaussian noise leads to the following problem:

$$y(i,j) = x(i,j) + n(i,j) \quad (1)$$

Here, additive noise is specified as $n(i,j)$, the image without noise is given as $x(i,j)$ and the noisy measurement is mentioned as $y(i,j)$. The role of de-noising $y(i,j)$ and estimating $\hat{x}(i,j)$ of $x(i,j)$ are too compulsory in this stage to lessen the MSE and hence these processes are given much attention. It is thus specified as,

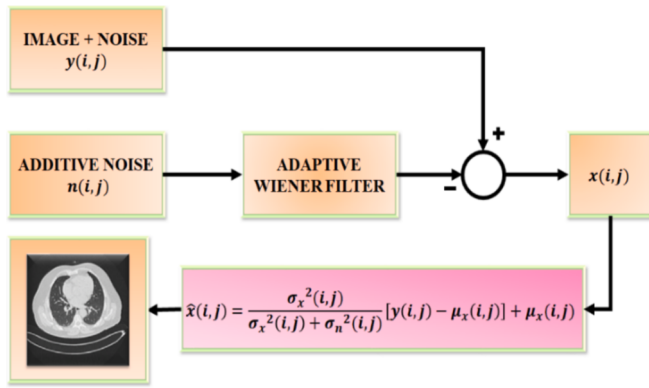


Fig. 2. Adaptive Wiener Filter Operation.

$$MSE(\hat{x}) = \frac{1}{N} \sum_{i,j=1}^N (\hat{x}(i,j) - x(i,j))^2 \quad (2)$$

Here, N specifies the number of elements in (i,j) .

The Wiener filter shows a simple scalar form when the $x(i,j)$ is a white Gaussian process, which is significantly represented as,

$$\hat{x}(i,j) = \frac{\sigma_x^2(i,j)}{\sigma_x^2(i,j) + \sigma_n^2(i,j)} [y(i,j) - \mu_x(i,j)] + \mu_x(i,j) \quad (3)$$

Here, signal means and variances are respectively specified as μ and σ^2 whereas the mean value of noise is assumed as zero. The operation of Adaptive wiener filter in denoising the input image is remarkably portrayed in Fig. 2.

In general, an uniform moving average window of size $(2r+1) \times (2r+1)$ is used for computing the local variance and means, which is specified as,

$$\hat{\mu}_x(i,j) = \frac{1}{(2r+1)^2} \sum_{p=i-r}^{i+r} \sum_{q=j-r}^{j+r} y(p,q) \quad (4)$$

$$\hat{\sigma}_x^2(i,j) = \frac{1}{(2r+1)^2} \sum_{p=i-r}^{i+r} \sum_{q=j-r}^{j+r} (y(p,q) - \hat{\mu}_x(i,j))^2 - \sigma_n^2 \quad (5)$$

For estimating $\hat{\sigma}_x^2(i,j)$, the weighted form of equation (5) is used as,

$$\hat{\sigma}_x^2(i,j) = \sum_{p=i-r}^{i+r} \sum_{q=j-r}^{j+r} w(i,j,p,q) (y(p,q) - \hat{\mu}_x(i,j))^2 \quad (6)$$

In the process of estimating the nonstationary weights $w(i,j,p,q)$ for an image with unexpected edges, the implementation of adaptive techniques is highly essential for choosing $w()$. Hence, the pixels, which are applied for computing the local variance σ^2 of (i,j) has to be biased in correspondence to the pixels having similar values of $y(i,j)$. It is significantly specified as,

$$w(i,j,p,q) = \frac{K(i,j)}{1 + a(\max[\epsilon^2, (y(i,j) - y(p,q))^2])} \quad (7)$$

Here, $K(i,j)$ specifies the normalization constant and $w(i,j,p,q)$ is set as zero. It is thus expressed as,

$$K(i,j) = \left\{ \sum_{p,q} \frac{1}{1 + a(\max[\epsilon^2, (y(i,j) - y(p,q))^2])} \right\}^{-1} \quad (8)$$

The weight function's parameters are given as $\epsilon = 2.5\sigma_n$ and $a > 0$. For excluding the outliers from weight function $w()$, the parameter is selected as $a\epsilon^2 \gg 1$. Therefore, the local mean and variance are estimated through $w()$ as,

$$\hat{\mu}_x(i,j) = \sum_{p=i-r}^{i+r} \sum_{q=j-r}^{j+r} w(i,j,p,q) y(p,q) \quad (9)$$

$$\hat{\sigma}_x^2(i,j) = \sum_{p=i-r}^{i+r} \sum_{q=j-r}^{j+r} w(i,j,p,q) (y(p,q) - \hat{\mu}_x(i,j))^2 \quad (10)$$

Thus, the effective estimation of σ_x^2 and μ_x significantly enhances the performance near edges, which in turn efficiently pre-processes the image by eliminating the unwanted noises or disruptions. The processed output is then given as the input to the next phase called segmentation.

3.2. Image segmentation

The pre-processed image is then segmented into multiple divisions with the assistance of the proposed Cascaded KM-FCM algorithm, which owns plenty of beneficial impacts like maximum reliability, quick convergence and less complexity since it is a combination of both Fuzzy C Means and K means algorithms. This algorithm couples the concept of FCM algorithm, which permits each data to be simultaneously allocated to multiple clusters through various membership degrees and the data variance concept of KM algorithm that is used for the data allocation to the cluster center.

For describing the Cascaded KM-FCM algorithm, the image with $X \times Y$ pixel resolution has to be segmented into multiple divisions n_c . Hence, the j^{th} center is specified as j whereas the input pixel, which has to be segmented is specified as $p(x,y)$ and so the overall segmentation using this algorithm is significantly expressed in the subsequent section.

1 Set the centers by utilizing the following formulation as

$$C_j = \min_{p(x,y)} + (2j-1) \left(\frac{\max_{p(x,y)} - \min_{p(x,y)}}{2n_c} \right) \quad (11)$$

Here, maximum and minimum intensity of image pixels are respectively specified as $\max_{p(x,y)}$ and $\min_{p(x,y)}$.

2 Fix the values of small constants as α_b and α_a as 0.05, where $\alpha_a = \alpha_0$

3 Compute the Euclidean distance (d) for every image pixels by applying the below mentioned formation as

$$d = \|p(x,y) - C_j\| \quad (12)$$

4 Allocate every pixels to the closest center on the basis of d and compute the centre locations as

$$C_j = \frac{1}{n_j} \sum_{y \in C_j} \sum_{x \in C_j} p(x,y) \quad (13)$$

5 Find out the difference between the center and members

$$\sigma^2(C_j) = \frac{1}{n_j} \sum_{y \in C_j} \sum_{x \in C_j} (p(x,y) - C_j)^2 \quad (14)$$

It aids in assessing the relation among the members and center.

6 Discover the centre, which has largest (C_l) and smallest (C_s) distance between the members and center

7 When $\sigma^2(C_s) < \alpha_a \sigma^2(C_l)$

- By computing the Euclidean distance among C_l and other centers, the closest centre (C_c) to C_l has to be identified.
- Allocate the members of C_l to the closest centre when $C_c < C_l$ whereas leave the remaining members to C_l when $x, y \in C_l$ and $p(x,y) < C_l$.
- Allot members of C_l to the closest centre when $C_c > C_l$ whereas leave the remaining members to C_l when $x, y \in C_l$ and $p(x,y) > C_l$.
- Re-compute the locations of C_c and C_l on the basis of the subsequent formation as,

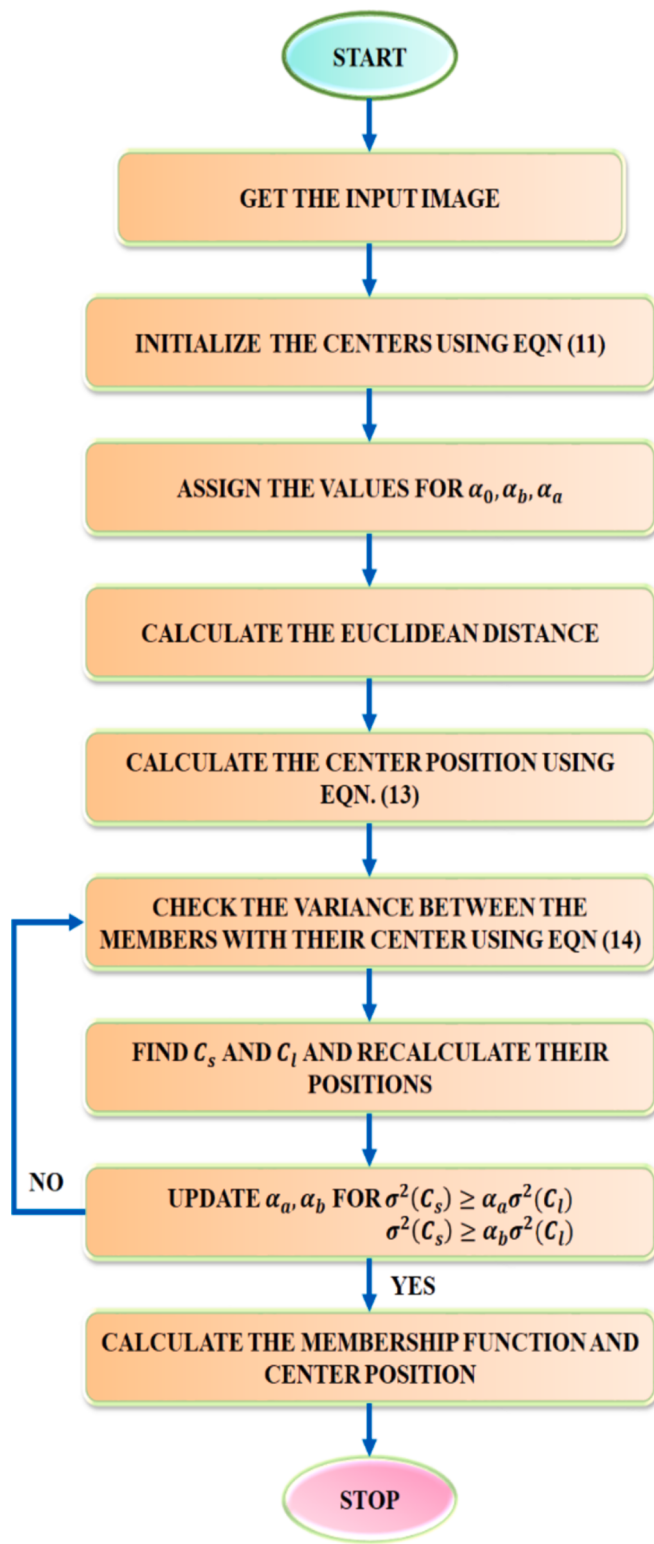


Fig. 3. Flow representation of Cascaded KM-FCM.

$$C_l = \frac{1}{n_l} \sum_{y \in C_l} \sum_{x \in C_l} p(x, y) \quad (15)$$

$$C_c = \frac{1}{n_c} \sum_{y \in C_c} \sum_{x \in C_c} p(x, y) \quad (16)$$

After the process in step 7d, the number of new members in C_c and C_l are mentioned as n_c and n_l .

8 Upgrade α_b and α_a on the basis of $\alpha_a = \alpha_a - \alpha_a/n_c$ or repeat 6 and 7 until $\sigma^2(C_s) \geq \alpha_a \sigma^2(C_l)$ is attained

9 Re-allocate every pixels to the closest centre and re-compute the centre locations through equation (13)

10 Upgrade α_b and α_a on the basis of $\alpha_a = \alpha_0$ and $\alpha_b = \alpha_b - \alpha_b/n_c$ or repeat steps 5–9 until $\sigma^2(C_s) \geq \alpha_b \sigma^2(C_l)$ is attained

11 Determine the membership function, $M_{jp(x,y)}$ through the subsequent equations as

$$M_{jp(x,y)} = 1 / \sum_{k=1}^{n_c} (d_{jp(x,y)} / d_{kp(x,y)})^2 \quad (17)$$

Where,

$$d_{jp(x,y)} = \|p(x,y) - C_j\| \text{ and } d_{kp(x,y)} = \|p(x,y) - C_k\| \quad (18)$$

$$\left. \begin{array}{l} M_{kp(x,y)} = 1 \\ M_{jp(x,y)} = 0; \text{ for } p(x,y) \neq k \end{array} \right\} \text{ if } d_{kp(x,y)} = 0 \quad (19)$$

12 Compute the center location through the following formation as

$$C_j = \sum_{y \in C_j} \sum_{x \in C_j} M_{jp(x,y)}^2 p(x,y) / \sum_{y \in C_j} \sum_{x \in C_j} M_{jp(x,y)}^2 \quad (20)$$

In order to describe the functioning measures of Cascaded KM-FCM algorithm in segmenting the image, the flow of these steps are clearly portrayed in Fig. 3.

Through the effective implementation of all these steps, the segmentation of the given image is significantly carried out with optimal reliability and these segmented images are then provided to the next stage for optimal image extraction.

3.3. Radiomic feature extraction

The term radiomics describes the identification of unique diagnostic and prognostic features of cancer imaging data in an automatic manner. By converting standard-of-care medical images into quantitative image data, which is consequently analysed by adopting different approaches like artificial intelligence, conventional biostatics and machine learning approaches. The extracted features from the medical images are further compared with the end point data for attaining enhanced prediction. By providing a Decision Support System (DSS), the radiomics supports clinical decisions along with the diagnosis in an accurate manner. DSS integrates radiomics features offering a holistic view of the patient's condition, enabling the identification of patterns or correlations. DSS also utilizes these features to provide diagnostic support, helping to identify the presence of disease, its stage and its characteristics with greater accuracy. The extracted radiomics features include features based on texture, wavelet, shape and first-order statistics. The grey level intensity's features like range, maximum, minimum, mean, kurtosis and skewness are extracted. The working measures of this Radiomic approach is clearly demonstrated in Fig. 4.

The variation in intensity related features that redirects the homogeneity of Region of Interest (ROI) and uniformity is evaluated for every gray value through sum of squares.

$$\text{Uniformity} = \sum_{i=1}^{N_g} (p(i))^2 \quad (21)$$

Where, the term $p(i)$ and N_g refers to the histogram of normalized intensity and discretized gray-level intensity. The histogram of first-

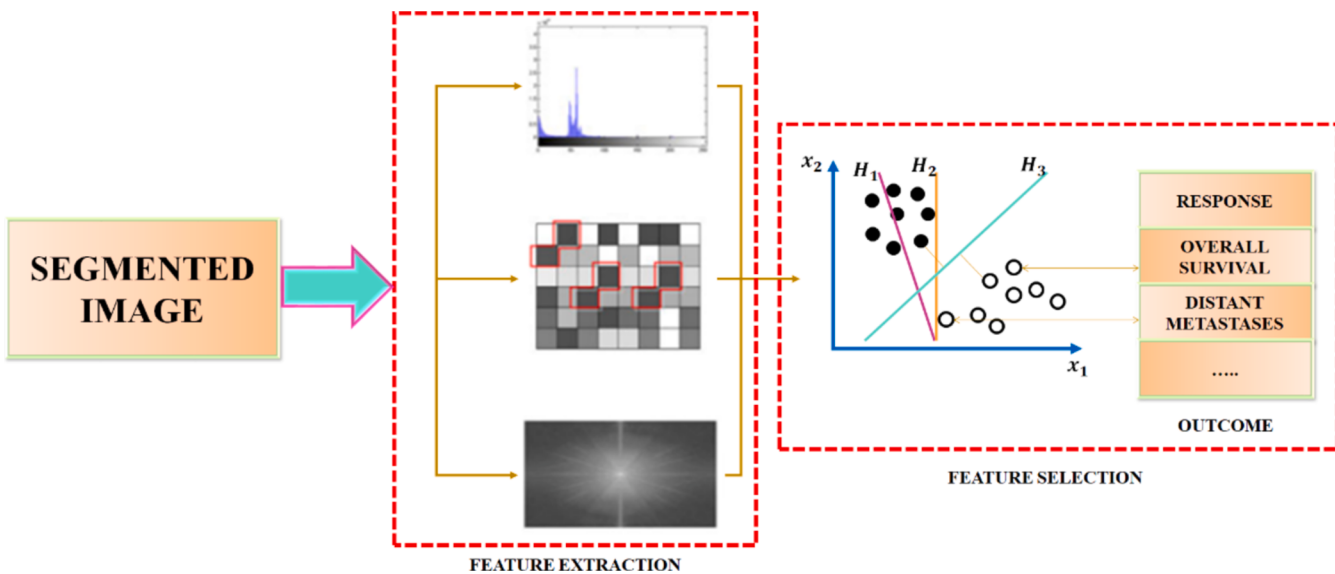


Fig. 4. Feature Extraction and Selection Using Radiomic.

order gray-level is given by,

$$h(i) = \sum_{X=0}^{N-1} \times \sum_{Y=0}^{M-1} \delta(f(x, y), i) \quad (22)$$

Where, the image magnitude is represented by the terms N and M . The Kronecker delta function and pixel value is denoted by the terms δ and i respectively. For the radiomic features that are extracted, the value of intensity level average is defined as mean and the disparities that exist around the averages is defined as variance. Subsequently, the skewness feature refers to the histogram shape or symmetrical curve distortion for the selected data set. Positive skewness suggests that the majority of the pixel values are relatively low, with fewer pixels having higher intensities whereas negative skewness implies that while most of the pixel values are high, there are a few significantly lower intensity pixels. The histogram flatness and consistency are defined by the terms Kurtosis and Entropy respectively. Based on the image's modality, the variation in pixel standard takes place. The Cluster Prominence (CP) is represented as,

$$CP = \sum_{i=1}^{Ng} \times \sum_{j=1}^{Ng} (i + j - u_x - u_y)^4 p(i, j) \quad (23)$$

After the image is given as input, the evaluation of Gray-Level Co-occurrence Matrix (GLCM) takes place, in which sum of the amount of definite pixel value j , which is d distance away from i is determined. A feature sample known as energy is obtained with the assistance of GLCM, which is provided as

$$E = \sum_i \{p(i, j)\}^2 \quad (24)$$

For every image, the evaluation of run length feature is done. A lossless data compression approach, which compresses the data by minimizing runs of data that are repetitive and sequential is known as Run-length encoding (RLE). The application of RLE for imaging is crucial to fulfil the need of storing the recurrent adjacent pixels in new field. The volume and density of the tumour is evaluated by the determination of surface area, spherical ratio, compactness, etc. The magnitude of compactness is given as,

$$\text{Compactness} = \frac{V}{\sqrt{\pi A^2}} \quad (25)$$

Where, the terms V and A refer to the volume and area of ROI respectively. The shape parameters relies on tumour mask, which aids in

the removal of ROI. The process of feature selection takes place after the process of feature extraction is complete.

3.4. Radiomic feature selection

The feature selection is chief process of radiomic feature determination, which aids in the robust identification of hidden data concepts and elimination of data over-fitting by reducing the amount of features extracted to a few patterns. Over-fitting is a consequence of high level of complexity (large number of features). In machine learning, the concept of over-fitting is an issue since the analysis delivers exceptional results on training data and underperforms on new test data. This issue is overcome by the approaches like early stopping learning process and cross-validation, which assist in significantly reducing the amount of features. The approaches used for selecting the features are Mutual Information (MI), Pearson Correlation Coefficient (PCC) and Analysis of Variance (ANOVA) whereas the most meaningful features are chosen using the set theorem.

3.4.1. Mutual information

The MI is very effective in measuring the correlation between features, which indicates the uncertain nature of features corresponding to one another. Consider two random variables X and Y . The MI $I(X, Y)$ between these two random variables estimates the quantity of information about X present in Y and vice versa. The $I(X, Y)$ is considered as an appropriate consistency measure among the measurements made by various observers. In MI, the selection of features is performed by evaluating the mutual dependence between two features and is given by,

$$I(X, Y) = \sum_{i,j} p(x_i, y_j) \log \frac{p(x_i, y_j)}{p(x_i)p(y_j)} \quad (26)$$

Here, $p(x_i, y_j)$ represents the joint probability mass and $p(x_i), p(y_j)$ represents the marginal probability mass. The MI is calculated between two discrete variables by partitioning the complete sample space into various sub regions, in which the samples are uniformly distributed. By using the chi-square statistic, the uniformity of the sample distribution is tested and the chi-square statistic is given by,

$$\chi^2 = \sum_{i=1}^n \sum_{j=1}^m \frac{(N(x_i, y_j) - E(x_i, y_j))^2}{E(x_i, y_j)} \quad (27)$$

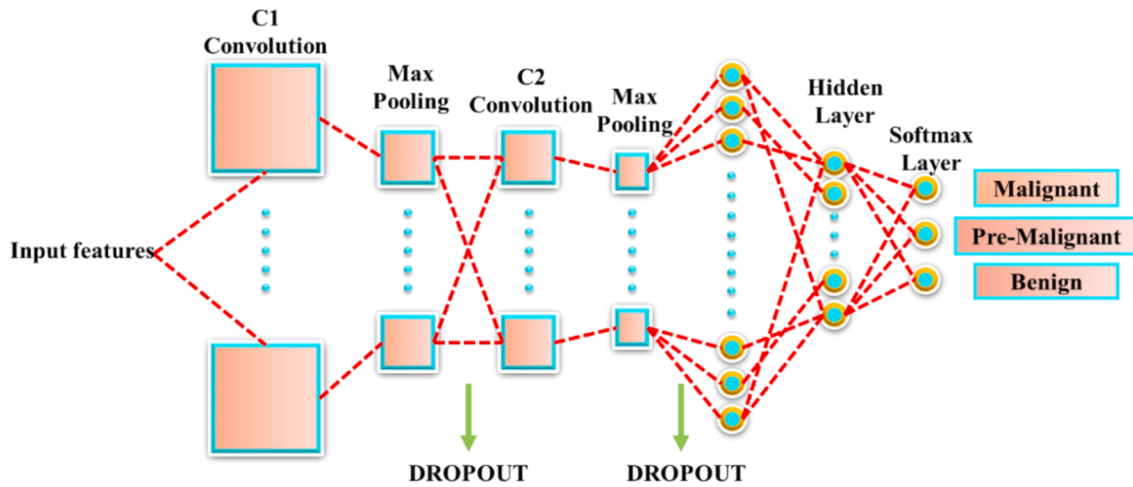


Fig. 5. Structure of CNN.

Table 1
CNN hyper-parameters.

Hyper-parameters	Description
Batch size	64
Number of epochs	5
Number of convolutional layers	2
Number of pooling layers	2
Intermediate layer's activation function	ReLU
Output layer's activation function	Softmax

Here, $E(x_i, y_j)$ indicate the expected number of uniformly distributed samples. The subspace is partitioned further if the samples are not uniformly distributed.

3.4.2. Pearson correlation Coefficient

In PCC, the selection of features is performed by evaluating the linear connection strength between two variables. It performs the evaluation of various feature subsets depending on the highly correlated features and removes the redundant ones. The merit M for the feature subset of the feature vector (FV) containing i features is indicated as,

$$M_{FVi} = \frac{i \times avg_{cf}}{\sqrt{i + i(i - 1)avg_{ff}}} \quad (28)$$

Here, avg_{ff} denotes the correlations of feature-feature and avg_{cf} denotes the correlations of feature-classification. The PCC based feature extraction criterion is expressed as,

$$PCC - FS = \max_{FVi} \left[\frac{avg_{cf_1} + avg_{cf_2} + \dots + avg_{cf_i}}{\sqrt{i + 2(avg_{f_1}f_k + \dots + avg_{f_m}f_n + \dots + avg_{f_1}f_1)}} \right] \quad (29)$$

Here, $avg_{f_m}f_n$ and avg_{cf_i} indicate the correlations among the continuous features. If W_i denote the complete feature vector with F_i features, the optimized feature vector related to PCC is given by,

$$PCC - FS = \max_{FVi} \left[\frac{\left(\sum_{j=1, k=1}^i f_j w_i \right)^2}{\sum_{j=1}^i w_i + \sum_{j \neq k} 2 \times f_j w_j w_{ij}} \right] \quad (30)$$

The redundant vectors are termed as the features with high correlation value and hence the features with minimum redundancy between consecutive features are selected.

3.4.3. ANOVA

ANOVA evaluates the distinctness of each features and further minimizes the feature dimensionality. It analyses the experimental data and measures one or more response variables for different conditions. ANOVA also compares the response variable means for different classification variable combinations. Using these three approaches, the feature set size is minimized and quick detection of cancer is ensured. In the context of radiomics feature extraction, ANOVA is particularly useful for assessing whether the variation in radiomics features across different groups is greater than the variation observed within these groups. This helps in identifying features that effectively distinguish between conditions or categories. Initially, ANOVA examines the impact of one or more factors by comparing the means of different groups and assessing whether the observed differences are greater than what would be expected by chance. Further, ANOVA performs the estimation of variance analysis measuring the variability of data within each group. The F-statistic is then determined by ANOVA as the ratio of the variance within groups to the variance between groups. An elevated F-statistic implies that there is a difference between the groups concerning the feature under examination. The following provides the sample variance between groups:

$$s_B^2(\xi) = \sum_{i=1}^K m_i \left(\frac{\sum_{j=1}^{m_i} f_{\xi}^g(i, j)}{m_i} - \frac{\sum_{i=1}^K \sum_{j=1}^{m_i} f_{\xi}^g(i, j)}{\sum_{i=1}^K m_i} \right)^2 / df_B \quad (31)$$

The sample variance within groups is given by,

$$s_w^2(\xi) = \sum_{i=1}^K \frac{m_i}{m_i} \left(\frac{\sum_{j=1}^{m_i} f_{\xi}^g(i, j)}{m_i} - \frac{\sum_{i=1}^K \sum_{j=1}^{m_i} f_{\xi}^g(i, j)}{\sum_{i=1}^K m_i} \right)^2 / df_w \quad (32)$$

Here, $df_B = K - 1$ is the degree of freedom for mean square between and $df_w = M - K$ is the degree of freedom for mean square within, K indicates number of groups, M indicates number of samples and m_i indicates number of samples in i^{th} group. Now, the ANOVA score is defined by,

$$S(\xi) = \frac{s_B^2(\xi)}{s_w^2(\xi)} \quad (33)$$

The larger value of $S(\xi)$ denotes better discriminative capability of the ξ -th feature and the features are subsequently ranked according to the S values. The feature sets obtained from MI, PCC and ANOVA are further reduced by set theory which is utilized to choose the optimal set of features.

3.4.4. Set theory

In order to select meaningful features, initially, the set theory defines

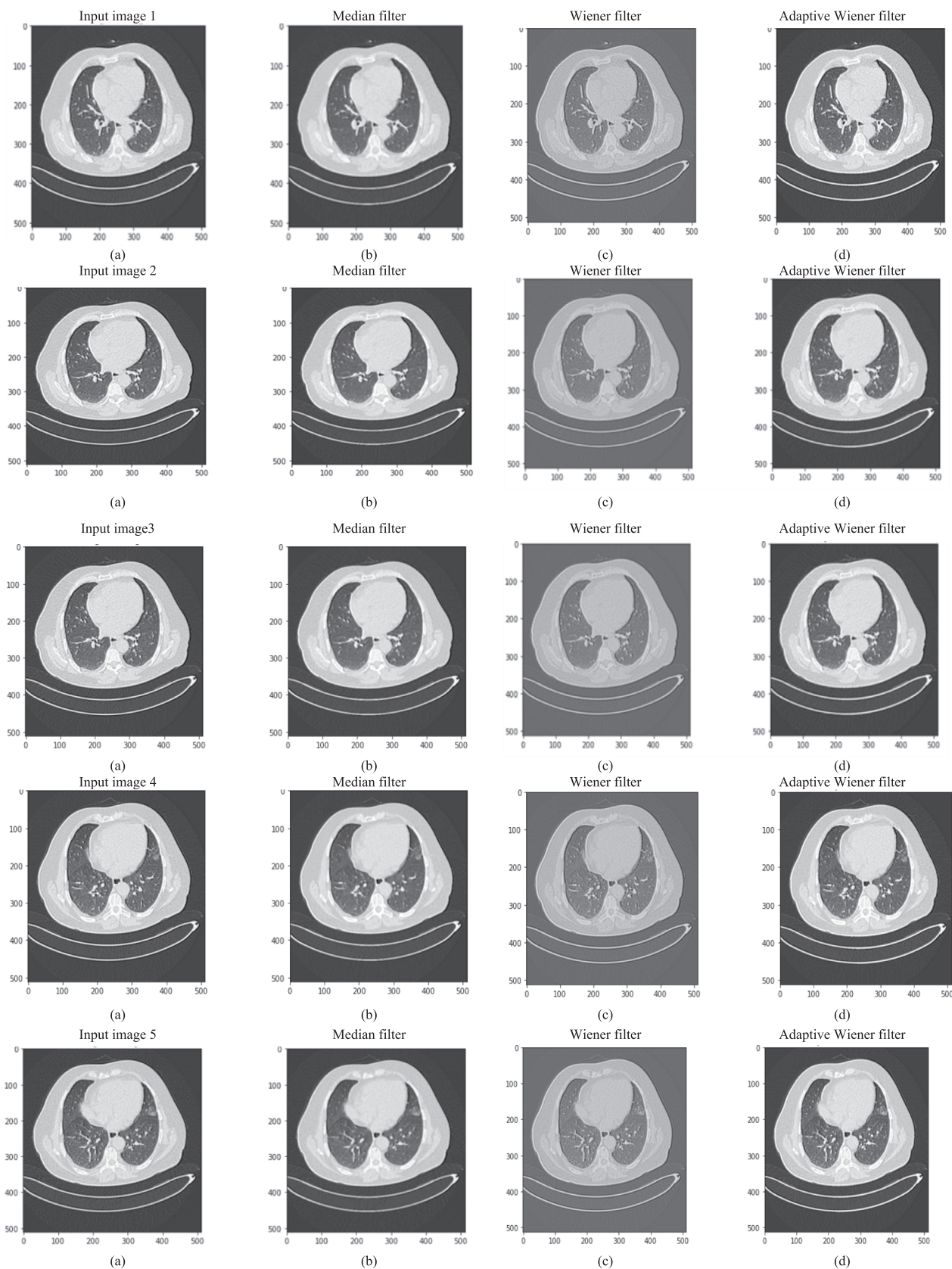
**Fig. 6.** Pre-processed image.

Table 2

Comparison of filters.

Parameters	Median filter	Wiener filter	Adaptive Wiener filter
PSNR	27.7791	31.3307	33.5201
SSIM	0.7936	0.9340	0.9556
MSE	108.4332	47.8632	42.7783
RMSE	10.4131	6.9183	4.8824

a decision table. Consider $T(U, P, C, D)$ as the decision table, in which U denotes universe of objects, P denotes the primitive feature set, C indicates the conditional attribute set, D denotes the class label or decision attribute and $C, D \subseteq P$. Considering the arbitrary set $A \subseteq P$, the indiscernibility relation is given by,

$$IND(A) = \{(x, y) \in U \times U : \forall q \in A, q(x) = q(y)\} \quad (34)$$

This relation is used to group objects in U that are indistinguishable based on a subset of attributes $A \subseteq P$. Objects that share the same values for all attributes in A are considered equivalent under this relation.

When $A \subseteq C$ and $X \subseteq U$, lower and upper approximations of X corresponding to A are mentioned as,

$$A_{low}X = \{x \in U : [x]_{IND(A)} \subseteq X\} \quad (35)$$

$$A_{high}X = \{x \in U : [x]_{IND(A)} \cap X \neq \emptyset\} \quad (36)$$

$$\text{Here, } [x]_{IND(A)} = \{y \in U : q(y) = q(x), \forall q \in A\} \quad (37)$$

All objects that certainly belong to a concept are included in the lower approximation, while objects that could possibly belong to it are included in the upper approximation. Equation (37) indicates the equivalent class of x in $U/IND(A)$. The set of all objects from the universe U denote the A – positive region of D and is given by,

$$POS_A(D) = \bigcup_{x \in U/IND(D)} A_{low}X \quad (38)$$

The dependency of D on A is given by,

$$\gamma_a(D) = \frac{|POS_A(D)|}{|U|} \quad (39)$$

The dependency function quantifies the extent to which the decision attribute D depends on the condition attributes A and is a measure of how well A can predict D . A feature $q \in C$ is considered as dispensable if $\gamma_q(D) = \gamma_{q-q}(D)$, q indicates an indispensable attribute in A corresponding to D . When all attributes are indispensable, an arbitrary set $E \subseteq C$ is termed as independent. Considering these factors, a reduct set of features are defined as $R \subseteq C$, when R is independent and $(D) = POS_C(D)$. Here, R is the reduct of C . The features like mean, uniformity, energy, surface area and depth are selected using MI, PCC and ANOVA approaches. Among these features, area and depth are the meaningful features selected by set theory since these features have outperformed others in the prediction of tumour. This approach is simple and it reduces the complexity of the operation. The functions of set theory in lung cancer diagnosis are listed below.

- By selecting a subset of meaningful features from a larger set, set theory helps in reducing the complexity of the model.
- Meaningful features selected via set theory contribute more significantly to the predictive models' ability to accurately diagnose cancer. By focusing on features with higher discriminative power, the proposed model more effectively differentiates between cancerous and non-cancerous stages.
- Analyzing fewer, more relevant features speeds up the computational process. This efficiency is crucial for clinical settings, where timely diagnosis and treatment initiation can significantly affect patient outcomes.

- By identifying features that are most indicative of specific cancer characteristics, set theory aids in improving treatment effectiveness and patient prognosis.

The obtained features have to be classified for the efficient detection of cancer and hence are applied to neural network based classifier.

3.5. Classification by Locust assisted crow search optimized CNN

CNN is one of the most often applied deep learning techniques for effective image classification. The deep learning approaches include raw images and performs higher-level feature extraction by multiple layers in a progressive manner. The presence of more than one hidden layer that makes the deep learning network to function as similar as the human brain is termed as neural networks. These networks have a single input and output layer but number of hidden layers varies according to the designers' demand. In neural networks, each layer processes the input images and further delivers the outputs to the next layers. Until the output layer is reached, the process gets repeated and the predicted results are obtained in the output layer. Among various deep learning approaches, the CNN is widely opted. In a CNN architecture, the convolution, max pooling and sparse layers are present in between the input image and drop out. The architecture of CNN is illustrated in Fig. 5. In general, dropout layer is around 50% but the adoption of 60% dropout layer achieves the maximum classification accuracy with reduced overlearning.

The layers of CNN are significantly explained in the following section as,

- **Input layer:** Here, the raw images are received and then transferred to the subsequent layer for feature extraction.
- **Convolution layer:** The image features obtained by the implementation of filters are used for determining the testing stage matches. A convolution layer is defined by the equation below,

$$[f * g](t) = \int_0^{\tau} f(\tau)g(t - \tau)d\tau \quad (40)$$

Where, g and f refer to two functions in the range of $[0, t]$. The output size of convolution is given by,

$$\left[\frac{w - f + 2p}{s} \right] + 1 \quad (41)$$

- **Pooling:** The extracted features are then fed to pooling layer, in which only the essential parameters are secured by eliminating the negative features. The pooling layer input matrix is given by,

$$\left[\frac{I + 2p - 2}{s} \right] + 1 \quad (42)$$

- **Sparse layer:** This layer is composed of convolution layer. The results of this layer are combined and given to the succeeding layer.
- **Softmax layer:** This is the classifier's final layer and it performs the comparison of previous layer features with input features for the elimination of redundant features. The decimal probabilities of every class, which is used to determine n different classes is evaluated in this layer. The range of these values lies between 0 and 1. The features are secured in a column vector x .

$$p(y = j|x, \theta) = \frac{e^{\theta_j^T x}}{\sum_{j=1}^k e^{\theta_j^T x}} \quad (43)$$

Where the weight vector and target classes are represented by θ_j^T and k respectively.

The CNN adopts various hyper-parameters like number of convolution layers, number of pooling layers, number of dense layers, activation

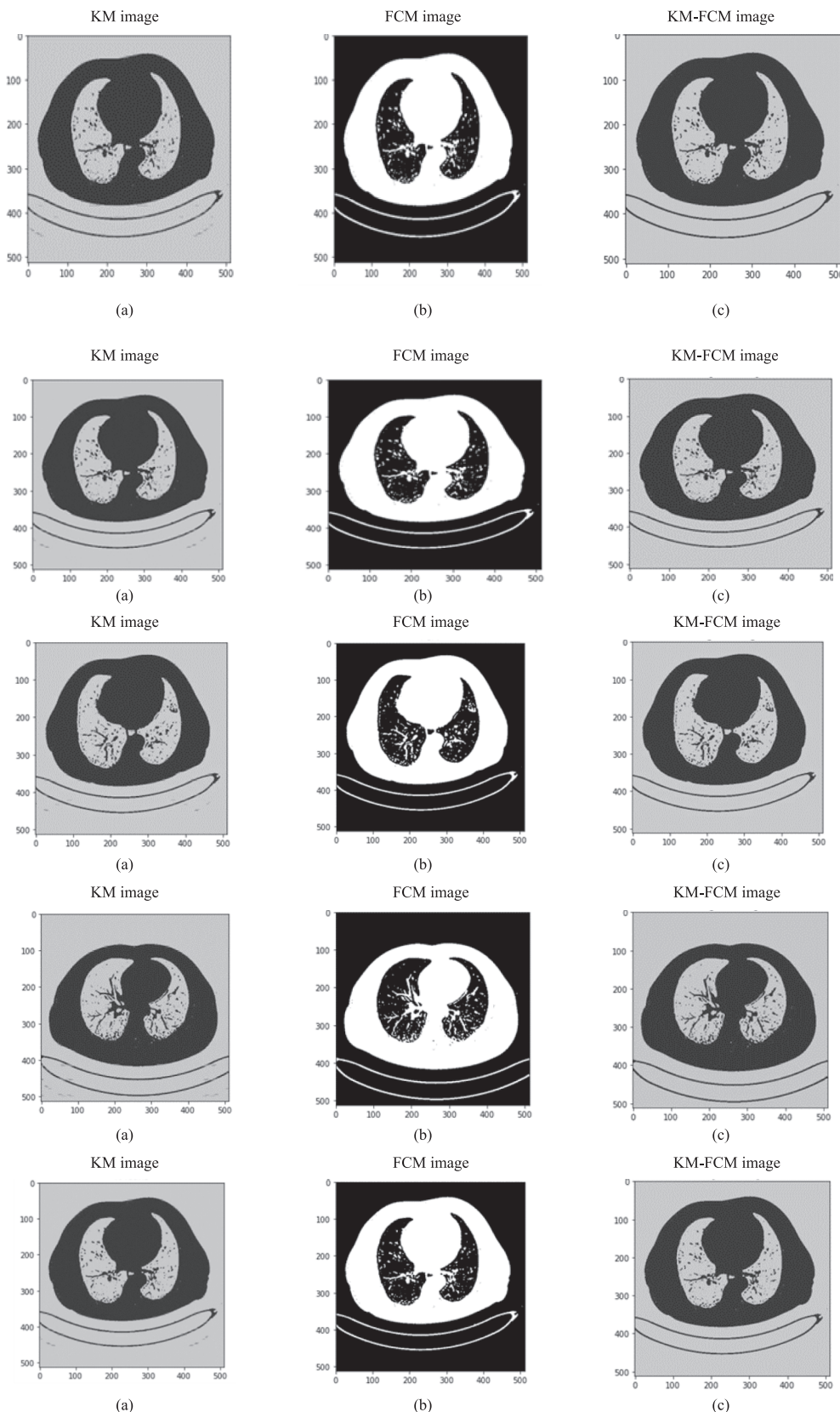
**Fig. 7.** Segmented image.

Table 3

Comparison of segmentation approaches.

Parameters	K-means	Fuzzy C means	KM-FCM
Normalized correlation	0.9957	0.005610	0.9968
Maximum difference	228.00	232.00	218.00
Average difference	0.0512	122.1352	0.0442
Normalized absolute error	0.0118	0.9948	0.0102

function, optimization function, batch size for iteration, number of epochs and loss function. In order to achieve better performance, these hyper-parameters must be combined correctly. The tuning of these hyper-parameters for selecting appropriate parameter values is very difficult. Hence, the nature-inspired algorithms are widely preferred for the tuning of hyper-parameters since these algorithms perform the significant reduction of search space and determine optimized solutions. This work proposes a novel locust assisted crow search algorithm with improved convergence rate, few control parameters and high efficiency for the optimization of CNN.

3.5.1. Locust assisted crow search algorithm

Generally, crows are considered smarter and clever in tool-making skills. The crows have the ability to recall faces easily and predicts the pilferer actions by using its own experience. Consider several crows in an environment, N indicates the number of crows and $X^{j,rept}$ ($j = 1, 2, \dots, N$, $rept = 1, 2, \dots, rept_{max}$) indicates the location of crow j in repetition ($rept$) search space. Here, $X^{j,rept} = [X_1^{j,rept}, X_2^{j,rept}, \dots, X_a^{j,rept}]$, $rept_{max}$ indicates the maximum number of repetitions. The position of the hiding place of crow j in $rept$ search space is indicated as $n^{j,rept}$. The crows perform the search operation by changing the position in order to find the better source of food. Due to the property of locust assisted at each generation, the crows change the positions. This change of position is carried out by a group of operators inspired by solitary phase and social phase. These phases are the two behavioural phases seen in desert locusts.

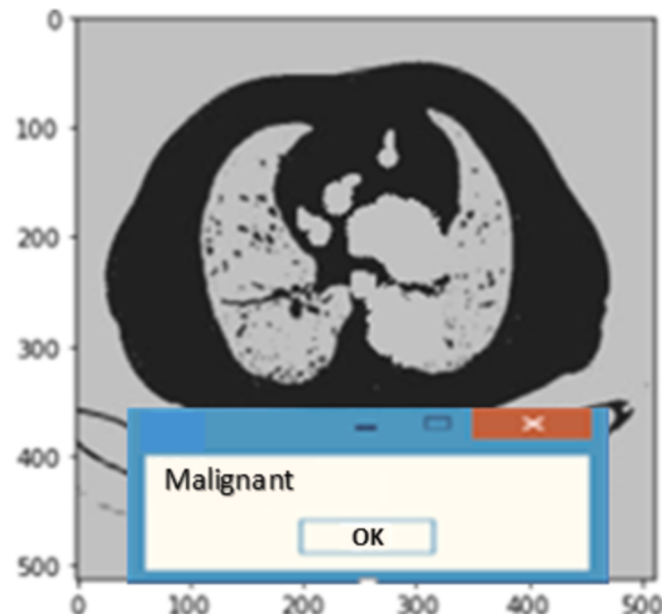
(i) Solitary phase

Here, the crows search for the promising food sources by moving in different locations but the crows do not mingle with other crows of the same species. The attraction and repulsion forces between the crows are considered in this phase. Hence, the total attraction and repulsion forces experienced by a particular crow i for any iteration k is given by,

Table 5

Reduced table.

IMAGES	AREA	DEPTH	RESULT
IMAGE 1	55.67	42.34	MALIGNANT
IMAGE 3	57.56	25.6	PREMALIGNANT
IMAGE 10	55.68	44.83	MALIGNANT
IMAGE 12	55.67	18.56	BENIGN
IMAGE 15	57.35	44.85	MALIGNANT
IMAGE 17	55.28	25.7	PREMALIGNANT
IMAGE 20	55.01	44.7	MALIGNANT

**Fig. 8.** Classification Outcome Using proposed CNN.**Table 4**

Features of lung cancer images.

IMAGES	MEAN	UNIFORMITY	ENERGY	SURFACE AREA	DEPTH	RESULT
IMAGE 1	2.6454	0.8589	4.7914	55.67	42.34	MALIGNANT
IMAGE 2	2.7844	0.8471	4.7109	56.07	23.42	PREMALIGNANT
IMAGE 3	2.8479	0.9289	4.7310	57.56	25.6	PREMALIGNANT
IMAGE 4	2.5694	0.8940	4.7257	50.98	48.75	MALIGNANT
IMAGE 5	2.3576	0.9013	4.7718	51.08	48.30	MALIGNANT
IMAGE 6	2.8759	0.8152	4.7017	54.06	16.71	BENIGN
IMAGE 7	2.5879	0.8931	4.7025	55.34	46.71	MALIGNANT
IMAGE 8	2.6987	0.8095	4.7354	53.79	18.55	BENIGN
IMAGE 9	2.9786	0.8913	4.7336	52.46	19.2	BENIGN
IMAGE 10	2.5487	0.8812	4.7923	55.68	44.83	MALIGNANT
IMAGE 11	2.5246	0.8246	4.7467	50.28	44.85	MALIGNANT
IMAGE 12	2.7567	0.8073	4.7065	55.67	18.56	BENIGN
IMAGE 13	2.5424	0.8359	4.7468	55.02	44.85	MALIGNANT
IMAGE 14	2.5032	0.8489	4.7358	51.78	44.85	MALIGNANT
IMAGE 15	2.1298	0.8016	4.7737	57.35	44.85	MALIGNANT
IMAGE 16	2.6098	0.8369	4.7374	55.28	54.3	MALIGNANT
IMAGE 17	2.8679	0.8957	4.7079	55.28	25.7	PREMALIGNANT
IMAGE 18	2.5108	0.9065	4.7358	51.08	44.8	MALIGNANT
IMAGE 19	2.8603	0.8467	4.7469	55.29	44.89	MALIGNANT
IMAGE 20	2.7018	6.7037	4.7729	55.01	44.7	MALIGNANT

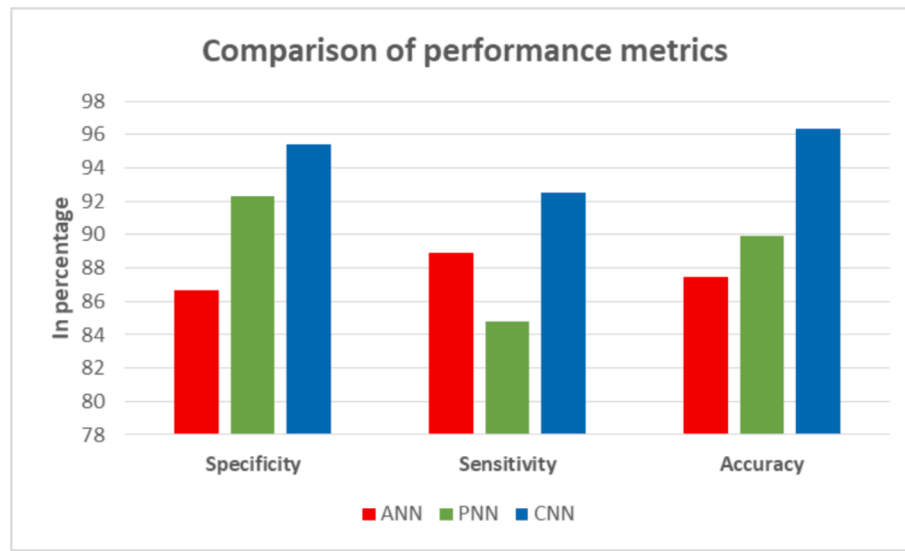


Fig. 9. Performance metrics comparison.

$$S_i^k = \sum_{\substack{j=1 \\ j \neq i}}^N s_{ij}^k \quad (44)$$

Here, s_{ij}^k represents the pairwise repulsion or attraction between the crow i and the crow j .

$$s_{ij}^k = \rho(c_i^k, c_j^k) s(r_{ij}^k) d_{ij} + \text{rand}(1, -1) \quad (45)$$

Here, $s(r_{ij}^k)$ indicates the social factor, in which r_{ij}^k denotes Euclidean distance between crows i and j . The distance is given by $r_{ij}^k = \|c_i^k - c_j^k\|$ and $\rho(c_i^k, c_j^k)$ indicates the dominance value between c_i^k and c_j^k . Hence $d_{ij} = (c_j^k - c_i^k)/r_{ij}^k$ represents the unit vector pointing from c_i^k to c_j^k and $\text{rand}(1, -1)$ represents the random vector, in which the elements are obtained from the uniform distribution of $[-1, 1]$.

$$s(r_{ij}^k) = M e^{-r_{ij}^k/L} - e^{-r_{ij}^k} \quad (46)$$

The parameters M and L indicate the magnitude and length scale of attraction or repulsion. For applying the operator $\rho(c_i^k, c_j^k)$, it is assumed initially that every individual $c_i^k \in C^k(c_1^k, c_2^k, \dots, c_N^k)$ is ranked with 0 indicating best individual to $N-1$ indicating worst individual. Hence, the dominance value is represented as,

$$\rho(c_i^k, c_j^k) = \begin{cases} e^{-(\text{rank}(c_i^k)/N)} & \text{if } \text{rank}(c_i^k) \leq \text{rank}(c_j^k) \\ e^{-(\text{rank}(c_j^k)/N)} & \text{if } \text{rank}(c_i^k) > \text{rank}(c_j^k) \end{cases} \quad (47)$$

Therefore, each crow i possess the tendency to move towards or away from other members by the influence of S_i^k . The updated position gained by the crow i is given by,

$$C_i^* = C_i^k + S_i^k \quad (48)$$

The solitary movement operators are applied to each crow $c_i^k \in C^k$ and a new set of candidate solutions $C^* = \{c_1^*, c_2^*, \dots, c_N^*\}$ are obtained. It denotes obtained position of each crow by the influence of other crows in the population.

(ii) Social phase

This operation is applied for refining certain best candidate solutions

$C^* = \{c_1^*, c_2^*, \dots, c_N^*\}$, which are obtained from the solitary phase. Initially, a subset of solutions $S = \{s_1, \dots, s_q\}$ comprising of q best solutions within C^* is defined. Subsequently, a set of h random solutions $P^i = \{p_1^i, \dots, p_h^i\}$ is generated for the subspace $B_i \in S$ with limits,

$$B_{i,n}^{\text{lower}} = s_{i,n} - r \quad (49)$$

$$B_{i,n}^{\text{upper}} = s_{i,n} + r \quad (50)$$

Here, $B_{i,n}^{\text{lower}}$ and $B_{i,n}^{\text{upper}}$ denote lower and upper bounds of each subspace B_i at n^{th} dimension, $b_{i,n}$ indicates the n^{th} element from the solution s_i . The value of r is given by,

$$r = \frac{\sum_{n=1}^d (s_n^{\text{upper}} - s_n^{\text{lower}})}{d} \cdot \beta \quad (51)$$

Here, s_n^{upper} and s_n^{lower} indicate the upper and lower bounds at n^{th} dimension, d represents the total count of decision variables. In addition, $\beta \in [0, 1]$ denotes the scalar factor that modulates the size of B_j . The best solution from $C_i^* \in S$ and the corresponding h random solutions $(p_1^i, p_2^i, \dots, p_h^i)$ are assigned as the position for the crow i at $k+1$, which is the next iteration. Hence, it is expressed as,

$$c_i^{k+1} = \text{best}(c_i^*, p_1^i, p_2^i, \dots, p_h^i) \quad (52)$$

The social phase operator excludes any solution c_i^* , which is not grouped within the group of best solution S . Henceforth, the final update of position applied to each crow i within the population is given by,

$$c_i^{k+1} = \left\{ \begin{array}{l} \text{best}(c_i^*, p_1^i, p_2^i, \dots, p_h^i) \text{ if } c_i^* \in S \\ c_i^* \text{ if } c_i^* \notin S \end{array} \right\} \quad (53)$$

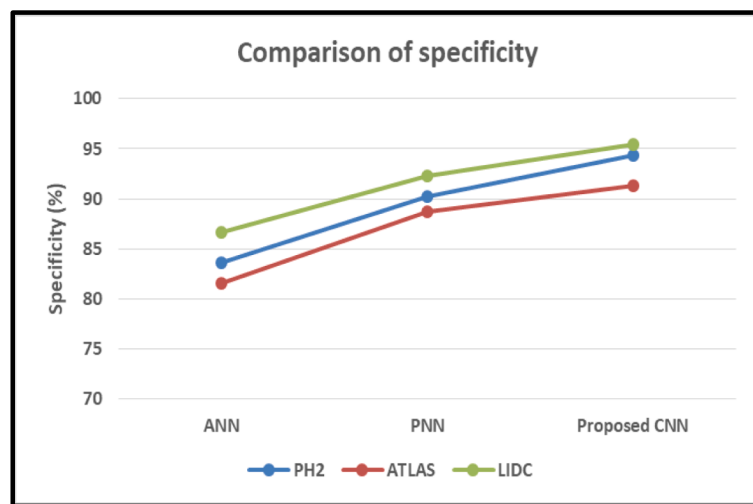
The steps involved in the novel Locust assisted Crow Search optimized CNN classification are explained as follows.

Step 1: Update the new location of the crow using equation (52).

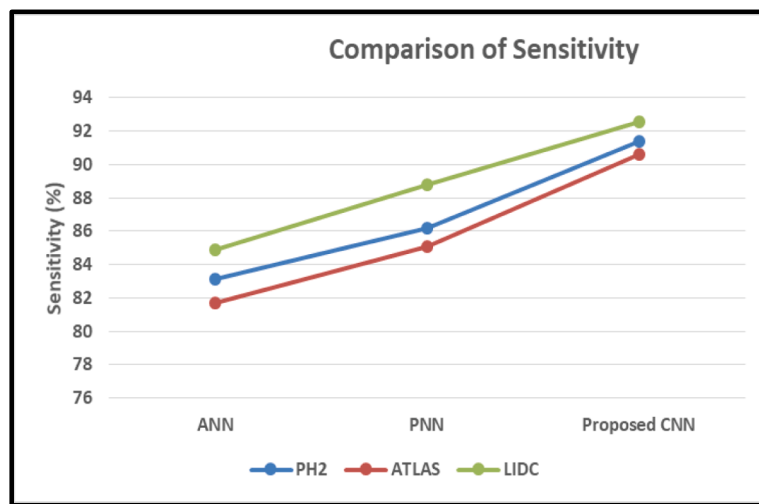
Step 2: Initialize the location as,

$$\text{Crows} = \begin{bmatrix} X_1^1 X_2^1 \dots X_a^1 \\ X_1^2 X_2^2 \dots X_a^2 \\ \vdots \\ X_1^N X_2^N \dots X_a^N \end{bmatrix} \quad (54)$$

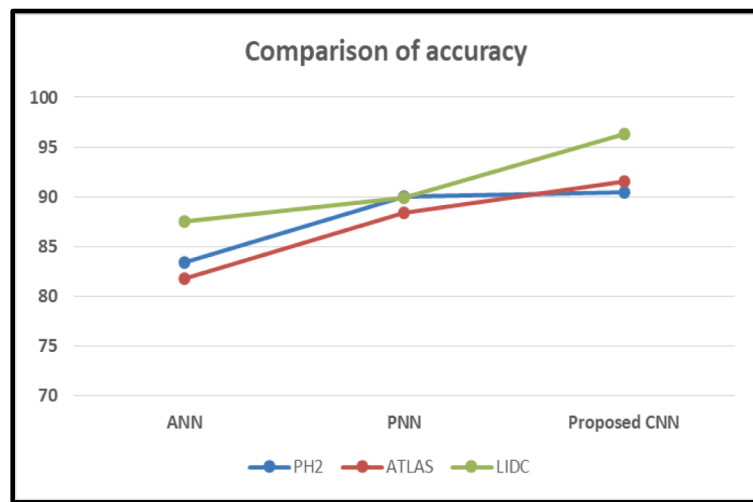
Step 3: Initialize the memory of each crow as,



(a)



(b)



(c)

Fig. 10. Graphical representation of performance metrics outputs.

Table 6

Comparison of performance metrics.

DATASET	NUMBER OF IMAGES USED	Specificity			Sensitivity			Accuracy		
		ANN	PNN	CNN	ANN	PNN	CNN	ANN	PNN	CNN
PH2	200	83.59	90.18	94.38	83.11	86.18	91.38	83.42	90.04	90.48
ATLAS	1012	81.50	88.66	91.26	81.70	85.06	90.6	81.80	88.36	91.57
LIDC	1018	86.65	92.33	95.42	84.88	88.78	92.55	87.5	89.92	96.33

$$\text{Memory} = \begin{bmatrix} mr_1^1 mr_2^1 \dots mr_a^1 \\ mr_1^2 mr_2^2 \dots mr_a^2 \\ \vdots \\ mr_1^N mr_2^N \dots mr_a^N \end{bmatrix} \quad (55)$$

Step 4: The crows establishes a new location in the search space. Consider that the crow i needs to identify a new location and hence a crow is selected randomly for observing the food caught by it. From equation (53), new location of the crow i is attained. Only if the location is stable, new location is updated or else the crow remains in its present location.

Step 5: Determine the fitness value (fit) of each crow's location and the memory of each crow.

$$mr^{i,rept+1} = \begin{cases} X^{i,rept+1} fit(X^{i,rept+1}) \geq fit(mr^{i,rept}) \\ mr^{i,rept}, \text{ otherwise} \end{cases} \quad (56)$$

Step 6: Repeat steps 4 and 5 till $rept_{max}$ is obtained. The best memory location corresponding to the objective function value is obtained as the optimized output.

To adjust CNN's hyper-parameters, the fitness values are utilised, and the dataset is trained based on the obtained hyper-parameters. In the context of hyperparameter tuning, the search space refers to all possible combinations of hyperparameters like the number of layers, batch size, activation functions, etc. The proposed algorithm adopting the combined behaviours of crows and locusts employs strategies to efficiently explore and exploit this space, focusing on promising areas more intensively. Following is the list of hyper-parameters selected by the Locust assisted CS approach.

Table 1 indicates the hyper-parameters adopted by proposed CNN. The initial convolutional layer comprises of 96 filters of [11 11] size with a stride value equal to 4 whereas the second convolutional layer has 10 filters of [5 5] size. The output of fully connected layer is 512. The dropout probability of dropout layer is about 0.1 and it enhances the generalization capability of the model. The final fully connected layer has the output size of 3 for the representation of three outputs. Finally, the Locust assisted CS based CNN classifier generates classified outputs of input images as malignant, pre-malignant and benign. Thus, it aids in providing efficient detection of lung cancer.

4. Results and discussion

This paper validates the proposed methodology using Python. The database used in this investigation was the Lung Image Database Consortium (LIDC), created by the National Cancer Institute (NCI). Around CT scans of 1018 patient records are included in this database. The images are categorized based on the growth of nodules. If the nodule growth is more, the condition is regarded as malignant.

The Lung Image Database Consortium (LIDC) dataset, used in this study, provides a diverse and well-represented collection of lung cancer cases. It includes a wide spectrum of nodule sizes, malignancy levels, and patient demographics, capturing both early-stage and advanced lung cancer cases. This diversity ensures that the model is trained on a broad variety of scenarios, which closely mirrors real-world clinical conditions.

Fig. 6 denotes the different sets of pre-processed images that are obtained from adaptive Wiener filter. The MSE between actual image

and the restored image is reduced by this filter generating better results. Moreover, high-frequency regions and edges of image are efficiently preserved by this filter, which is comparatively better than the median filter and Wiener filter.

Table 2 presents a comparison between the Adaptive Wiener filter and the Wiener filter and median filter with respect to the following metrics: MSE, RMSE, PSNR, and SSIM (Structural Similarity Index). The gathered outputs show that the suggested filter yields more accurate results with less error. The proposed Adaptive Wiener generates more precise filtering outputs with a reduced MSE value of 42.7783 and RMSE value of 4.8824. Consequently, the proposed filter generates improved PSNR and SSIM values of 33.5201 and 0.9556 respectively.

The obtained images after segmentation by KM, FCM and KM-FCM approaches for different set of images are given in Fig. 7. The segmentation of images is carried out by depending on the intensity, which in turn generates improved results. With this process, the infected region is segmented in an appropriate manner, which enables improved detection of lung cancer. The comparison of segmentation approaches in terms of different parameters is given in Table 3. On comparing with K-means and Fuzzy C means, it is visible that the KM-FCM approach produces improved results with a normalized correlation of 0.9968 and a normalized absolute error value of 0.0102. Moreover, the maximal and average difference values obtained are given by 218 and 0.0442 respectively.

The characteristics that are taken from the photos of lung cancer are shown in Table 4. It indicates features like mean, uniformity, energy, surface area and depth. The obtained outputs reveal the presence of different types of cancer like malignant, benign and premalignant. The images with increased depth value indicates malignant type and the images with reduced depth value indicates the benign type as shown in Table 5.

Fig. 8 represents the lung cancer detected image, which indicates the presence of malignant cancer. The proposed CNN classifier compares the features that are obtained from the extraction and selection process with the feature values of the trained data. The classifier records the trained data when any of the obtained feature matches the trained data. In this work, the tumour is classified as malignant, premalignant or benign.

Fig. 9 indicates the performance metrics comparison of the proposed CNN with Artificial Neural Networks (ANN) [39] and Probabilistic Neural Networks (PNN) [40]. While comparing the resultant values, the proposed CNN generates improved values of 95.42% specificity, 92.55% sensitivity and 96.33% accuracy as shown in Fig. 10.

Table 6 represents the comparison of proposed CNN with ANN and PNN in terms of the performance metrics like specificity, sensitivity and accuracy obtained from the datasets PH2, ATLAS and LIDC. The processing of images belonging to these datasets prove that the proposed CNN classifier generates improved performance. Moreover, the proposed approach performs the processing over more number of images from the LIDC dataset. Adopting more images indicate more comprehensive training data, leading to potentially more accurate and robust models. A larger dataset like LIDC allows for more exhaustive training and testing, which enhances the generalizability and reliability of the models developed. When compared to other datasets, more number of images is utilized from the LIDC dataset on which CNN generates an accuracy of 96.33 %, sensitivity of 92.55 % and specificity of 95.42 %.

5. Conclusion

The present study aims to achieve optimal accuracy in the process of detecting the occurrence of lung cancer through the effective implementation of image processing approach, in which the adaptive wiener filter is employed that involves in greatly lessening the amount of noise content in input image. The pre-processed image is then significantly segmented into various regions through the implementation of cascaded KM-FCM algorithm and the relevant features from the segmented images are effectively extracted by employing the radiomics approach. Eventually, the proposed Locust assisted CS based CNN classifier involves in classifying the images in consideration with the trained data base in an effective manner, which assists in identifying the types and stages of lung cancer with optimal accuracy. The entire work is validated in Python and the outcomes are evidently provided with prior analysis, which proves that the proposed approach delivers enhanced outputs with extreme accuracy of 96.33%, specificity of 95.42% and sensitivity of 92.55%. Moreover, the filtering outputs indicate minimized error values of 42.7783 MSE and 4.8824 RMSE. According to the results of the comparison, the proposed methodology outperforms several existing approaches.

Future work includes validating the model on larger and more diverse datasets to improve generalizability and robustness. Additionally, integrating multi-modal data, such as PET scans and patient demographics, is considered to enhance diagnostic accuracy. Efforts are directed towards improving model interpretability by employing techniques like saliency maps, allowing clinicians to understand the model's decisions. Optimization for real-time clinical implementation is prioritized by reducing computational complexity. Handling ambiguous cases through uncertainty quantification and developing hybrid models combining traditional and deep learning techniques are also potential avenues to further enhance the system's performance and reliability in clinical settings.

Declaration of competing interest

The authors declare that they have no known competing financial interests or personal relationships that could have appeared to influence the work reported in this paper.

Data availability

The authors do not have permission to share data.

References

- [1] T.I.A. Mohamed, A.-E.-S. Ezugwu, Enhancing Lung Cancer Classification and Prediction With Deep Learning and Multi-Omics Data, *IEEE Access* 12 (2024) 59880–59892, <https://doi.org/10.1109/ACCESS.2024.3394030>.
- [2] A. Wehbe, S. Dellepiane, I. Minetti, Enhanced Lung Cancer Detection and TNM Staging Using YOLOv8 and TNM Classifier: An Integrated Deep Learning Approach for CT Imaging, *IEEE Access* 12 (2024) 141414–141424, <https://doi.org/10.1109/ACCESS.2024.3462629>.
- [3] Y. Hussain Ali, V.S. Chooralil, K. Balasubramanian, R.R. Manyam, S.K. Raju, A. T. Sadiq, A.K. Farhan, Optimization system based on convolutional neural network and internet of medical things for early diagnosis of lung cancer, *Bioengineering* 10 (3) (2023) 320, <https://doi.org/10.3390/bioengineering10030320>.
- [4] P. Sathe, A. Mahajan, D. Patkar, M. Verma, End-to-End Fully Automated Lung Cancer Screening System, *IEEE Access* 12 (2024) 108515–108532, <https://doi.org/10.1109/ACCESS.2024.3435774>.
- [5] M. Imran, B. Haq, E. Elbasi, A.E. Topcu, W. Shao, Transformer-Based Hierarchical Model for Non-Small Cell Lung Cancer Detection and Classification, *IEEE Access* 12 (2024) 145920–145933, <https://doi.org/10.1109/ACCESS.2024.3449230>.
- [6] M. Magdy Amin, A.S. Ismail, M.E. Shaheen, Multimodal Non-Small Cell Lung Cancer Classification Using Convolutional Neural Networks, in: *IEEE, Access* 12 (2024) 134770–134778, <https://doi.org/10.1109/ACCESS.2024.3461878>.
- [7] A. Moradkhani, A. Broumandnia, S.J. Mirabedini, A portable medical device for detecting diseases using Probabilistic Neural Network, *Biomed. Signal Process. Control* 71 (2022) 103142, <https://doi.org/10.1016/j.bspc.2021.103142>.
- [8] N.F. Noaman, B.M. Kanber, A.A. Smadi, L. Jiao, M.K. Alsmadi, Advancing Oncology Diagnostics: AI-Enabled Early Detection of Lung Cancer Through Hybrid Histological Image Analysis, *IEEE Access* 12 (2024) 64396–64415, <https://doi.org/10.1109/ACCESS.2024.3397040>.
- [9] R. Gunawan, et al., Combining Multistaged Filters and Modified Segmentation Network for Improving Lung Nodules Classification, *IEEE J. Biomed. Health Inform.* 28 (9) (Sept. 2024) 5519–5527, <https://doi.org/10.1109/JBHI.2024.3405907>.
- [10] M.M. Mustafa, I. Manimozhi, T.R. Mahesh, S. Guluwadi, Optimizing double-layered convolutional neural networks for efficient lung cancer classification through hyperparameter optimization and advanced image pre-processing techniques, *BMC Med. Inf. Decis. Making* 24 (1) (2024) 142.
- [11] X. Ma, P. Wu, H. Shen, A nonlinear guided filter for polarimetric SAR image despeckling, *IEEE Trans. Geosci. Remote Sens.* 57 (4) (2018) 1918–1927, <https://doi.org/10.1109/TGRS.2018.2870188>.
- [12] H. Salehi, J. Vahidi, T. Abdeljawad, A. Khan, S.Y.B. Rad, A SAR image despeckling method based on an extended adaptive wiener filter and extended guided filter, *Remote Sens. (Basel)* 12 (15) (2020) 2371, <https://doi.org/10.3390/rs12152371>.
- [13] V. Gampala, V. Ramya, B. Maram, and S. Rao Pappu, Identification of lung cancer using archimedes flow regime optimization enabled deep belief network, *Multimedia Tools and Applications*, 1-30, 2024.
- [14] V. Göreke, A novel method based on Wiener filter for denoising Poisson noise from medical X-Ray images, *Biomed. Signal Process. Control* 79 (2023) 104031, <https://doi.org/10.1016/j.bspc.2022.104031>.
- [15] M. Salvi, A. Mogetta, U. Raghavendra, A. Gudigar, U. Rajendra Acharya, F. Molinari, A dynamic uncertainty-aware ensemble model: Application to lung cancer segmentation in digital pathology, *Appl. Soft Comput.* 165 (2024) 112081.
- [16] F. Zhao, Y. Chen, H. Liu, J. Fan, Alternate PSO-based adaptive interval type-2 intuitionistic fuzzy C-means clustering algorithm for color image segmentation, *IEEE Access* 7 (2019) 64028–64039, <https://doi.org/10.1109/ACCESS.2019.2916894>.
- [17] Z. Zhang, J. Song, An adaptive fuzzy level set model with local spatial information for medical image segmentation and bias correction, *IEEE Access* 7 (2019) 27322–27338, <https://doi.org/10.1109/ACCESS.2019.2900089>.
- [18] K.P. Sinaga, M.S. Yang, Unsupervised K-means clustering algorithm, *IEEE Access* 8 (2020) 80716–80727, <https://doi.org/10.1109/ACCESS.2020.2988796>.
- [19] S. Jardim, J. António, C. Mora, Graphical image region extraction with k-means clustering and watershed, *Journal of Imaging* 8 (6) (2022) 163, <https://doi.org/10.3390/jimaging08060163>.
- [20] Z. Zhou, S. Li, G. Qin, M. Folkert, S. Jiang, J. Wang, Multi-objective-based radiomic feature selection for lesion malignancy classification, *IEEE J. Biomed. Health Inform.* 24 (1) (2019) 194–204, <https://doi.org/10.1109/JBHI.2019.2902298>.
- [21] S.F.M. Radzi, M.K.A. Karim, M.I. Saripan, M.A. Abd Rahman, N.H. Osman, E. Z. Dahal, N.M. Noor, Impact of image contrast enhancement on stability of radiomics feature quantification on a 2D mammogram radiograph, *IEEE Access* 8 (2020) 127720–127731, <https://doi.org/10.1109/ACCESS.2020.3008927>.
- [22] U. Arif, C. Zhang, M. W. Chaudhary, and H. H. Khalid, Optimizing lung cancer prediction: leveraging Kernel PCA with dendritic neural models, *Computer Methods in Biomechanics and Biomedical Engineering*, pp. 1-14, 2024.
- [23] H. Liu, H. Li, M. Habes, Y. Li, P. Boimel, J. Janopaul-Naylor, Y. Xiao, E. Ben-Josef, Y. Fan, Robust collaborative clustering of subjects and radiomic features for cancer prognosis, *IEEE Trans. Biomed. Eng.* 67 (10) (2020) 2735–2744, <https://doi.org/10.1109/TBME.2020.2969839>.
- [24] T. S. Arulananth, L. Balaji, M. Baskar, V. Anbarasu, K. Srinivas Rao, PCA based dimensional data reduction and segmentation for DICOM images, *Neural Processing Letters* 55(1) (2023) 3–17. <https://doi.org/10.1007/s11063-020-10391-9>.
- [25] K. Tran, D. Ginzburg, W. Hong, U. Attenberger, and H. Soo Ko, Post-radiotherapy stage III/IV non-small cell lung cancer radiomics research: a systematic review and comparison of CLEAR and RQS frameworks, *European Radiology*, 1-17, 2024.
- [26] X. Xiao, Y. Qiang, J. Zhao, X. Yang, X. Yang, Segmentation of Liver Lesions without Contrast Agents with Radiomics-Guided Densely UNet-Nested GAN, *IEEE Access* 9 (2020) 2864–2878, <https://doi.org/10.1109/ACCESS.2020.3047429>.
- [27] C. Li, H. Chen, L. Zhang, N. Xu, D. Xue, Z. Hu, H. Ma, H. Sun, Cervical histopathology image classification using multilayer hidden conditional random fields and weakly supervised learning, *Ieee, Access* 7 (2019) 90378–90397, <https://doi.org/10.1109/ACCESS.2019.2924467>.
- [28] Q. Yin, J. Cheng, F. Zhang, Y. Zhou, L. Shao, W. Hong, Interpretable POLSAR image classification based on adaptive-dimension feature space decision tree, *IEEE Access* 8 (2020) 173826–173837, <https://doi.org/10.1109/ACCESS.2020.3023134>.
- [29] B. Liu, W. Guo, X. Chen, K. Gao, X. Zuo, R. Wang, A. Yu, Morphological attribute profile cube and deep random forest for small sample classification of hyperspectral image, *IEEE Access* 8 (2020) 117096–117108, <https://doi.org/10.1109/ACCESS.2020.3004968>.
- [30] S.B. Chaabane, M. Hijji, R. Harrabi, H. Seddik, Face recognition based on statistical features and SVM classifier, *Multimed. Tools Appl.* 81 (6) (2022) 8767–8784, <https://doi.org/10.1007/s11042-021-11816-w>.
- [31] N. Venkatesan, S. Pasupathy, B. Gobinathan, An efficient lung cancer detection using optimal SVM and improved weight based beetle swarm optimization, *Biomed. Signal Process. Control* 88 (2024) 105373.
- [32] S. U. Krishna, A. N. Lakshman, T. Archana, K. Raju, and M. Ayyadurai, Lung Cancer Prediction and Classification Using Decision Tree and VGG16 Convolutional Neural Networks, *The Open Biomedical Engineering Journal*, vol. 18, no. 1, 2024.
- [33] S. Wang, D.M. Yang, R. Rong, X. Zhan, J. Fujimoto, H. Liu, J. Minna, I.I. Wistuba, Y. Xi, G. Xiao, Artificial intelligence in lung cancer pathology image analysis, *Cancers* 11 (11) (2019) 1673, <https://doi.org/10.3390/cancers1111673>.
- [34] S. Pang, F. Meng, X. Wang, J. Wang, T. Song, X. Wang, X. Cheng, VGG16-T: a novel deep convolutional neural network with boosting to identify pathological type of

- lung cancer in early stage by CT images, International Journal of Computational Intelligence Systems 13 (1) (2020) 771–780, <https://doi.org/10.2991/ijcis.d.200608.001>.
- [35] L. Goel, S. Mishra, A hybrid of modified YOLOv3 with BBO/EE optimizer for lung cancer detection, Multimed. Tools Appl. 83 (17) (2024) 52219–52251.
- [36] S. Mammeri, M. Amroune, M.-Y. Haouam, I. Bendib, A.C. Silva, Early detection and diagnosis of lung cancer using YOLO v7, and transfer learning, Multimed. Tools Appl. 83 (10) (2024) 30965–30980.
- [37] K. Priyadarshini, M. Alagarsamy, K. Sangeetha, D. Thangaraju, Hybrid RNN-FFBPNN Optimized with Glowworm Swarm Algorithm for Lung Cancer Prediction, IETE J. Res. 70 (5) (2024) 4453–4468.
- [38] BR, Sampangi Rama Reddy, Sumanta Sen, Rahul Bhatt, Murari Lal Dhanetwal, Meenakshi Sharma, and Rohaila Naaz. “Stacked neural nets for increased accuracy on classification on lung cancer.” Measurement: Sensors 32 (2024): 101052.
- [39] I.M. Nasse, S.S. Abu-Naser, Lung cancer detection using artificial neural network, International Journal of Engineering and Information Systems (IJE AIS) 3 (3) (2019) 17–23, <https://doi.org/10.1109/IIEEEGCC.2011.5752535>.
- [40] S.C. Sr, H. Rajaguru, Lung cancer detection using probabilistic neural network with modified crow-search algorithm, Asian Pac. J. Cancer Prev. 20 (7) (2019) 2159.